The spectral analysis of the transitional millisecond pulsar J1023+0038

A Thesis

submitted to
Indian Institute of Science Education and Research Pune
in partial fulfillment of the requirements for the
BS-MS Dual Degree Programme

by

Shaswat Nair

Indian Institute of Science Education and Research Pune
Dr. Homi Bhabha Road,
Pashan, Pune 411008, INDIA.

May, 2023

Supervisor: Dr. Sudip Bhattacharyya

Certificate

This is to certify that this dissertation entitled The spectral analysis of the transitional millisecond pulsar J1023+0038 towards the partial fulfilment of the BS-MS dual degree programme at the Indian Institute of Science Education and Research, Pune represents study/work carried out by Shaswat Nair at Indian Institute of Science Education and Research under the supervision of Dr. Sudip Bhattacharyya, Professor, TIFR, Mumbai , during the academic year 2022-2023.

Dr. Sudip Bhattacharyya

Committee:

Dr. Sudip Bhattacharyya

Dr. Prasad Subramanian

This thesis is dedicated to my grandmother

Declaration

I hereby declare that the matter embodied in the report entitled The spectral analysis of the transitional millisecond pulsar J1023+0038 are the results of the work carried out by me at the TIFR, Mumbai, Indian Institute of Science Education and Research, Pune, under the supervision of Dr. Sudip Bhattacharyya and the same has not been submitted elsewhere for any other degree.

Shaswat Nair

Acknowledgments

I would like to thank Prof. Sudip Bhattacharyya for allowing me to conduct this project under his supervision. His guidance and mentorship have been crucial for the completion of my work. I would also like to thank Prof. Mayukh Pahari, without whose assistance in the XMM-Newton and XSPEC software, this project would not have been completed in this duration. I also thank Prof. Prasad Subramanian, my internal expert at IISER Pune, for his guidance and mentorship.

Abstract

PSR J102347.6 +003841 (also known as PSR J1023) is one of three known transitional millisecond pulsars (tMSP). We analyze EPIC X-ray data from the XMM-Newton satellite to probe multiple X-ray states of this star. By analyzing a combined total of 18 observations across multiple years, we hope to provide a comprehensive picture of the spectral properties of this source and analyze the effectiveness of various models in successfully describing its behavior. We perform the spectral fitting and modeling of the source using the spectral modeling software XSPEC and other tools within the publicly available Heasoft package.

Contents

Abstract **xi**

0.1 Neutron Stars 5

0.2 MSP Formation 6

0.3 The transitional millisecond pulsar 7

0.4 The history of J1023 7

0.5 The possible ellipticity of J1023 8

0.6 The scope of the project 9

1 Data files and Software **11**

1.1 The XMM-Newton EPIC Data 11

1.2 The XMM-Newton CCF 13

1.3 The XMM Science Analysis Software 14

1.4 HeaSoft 14

1.5 Miscellaneous 14

2 Data Analysis **17**

2.1 Setting up the XMMSAS environment 17

2.2 The MOS Analysis 19

2.3 Loading the files into XSPEC 24

3 Spectral Modeling and Fitting **25**

3.1 The Model 25

3.2 Fixed Parameters 26

4 Results **27**

4.1 The Spectral Fit 28

4.2 Calculations 30

4.3 Errors 30

4.4 Discussion 31

5 Conclusion and outlook **33**

List of Figures

1. Figure 2.1: Flowchart of MOS Data Analysis Pipeline
2. Figure 2.2: Visualisation of MOS data - source and background
3. Figure 2.3: Total co-added background subtracted lightcurve of Obs ID 0720030101
4. Figure 4.1: Spectral Fit of total MOS spectra

List of Tables

1. Table 1.1: Observation log of all XMM-Newton data used in the project
2. Table 1.2: Observation log (cont.d)
3. Table 4.1: Best-fit parameters of the spectral fit

Introduction

0.1 Neutron Stars

Neutron stars are one of the densest celestial objects currently known to us. They are the endpoints in the lives of stars with masses in the range of 10-25 solar masses having cores that exceed the Chandrashekhar limit [16]. When the cores of such massive stars begin to collapse, the electron degeneracy pressure of the core is overcome by its gravitational force, which compresses it to an extremely high degree. Under such high pressure, protons and electrons fuse to form neutrons, whose degeneracy pressure combined with strong force interactions halt the core's contraction [11]. The star's outer layers bounce off this highly dense core and are violently expelled outwards in a supernova [7]. During this process, the core retains most of its angular momentum while significantly shrinking in radius. This often results in newborn neutron stars having high spin periods, usually in the order of a few milliseconds. These objects are characterized by their high density and magnetization, which gives way to their classification into two broad categories -

1. Magnetars are neutron stars with nearly 1000 times stronger magnetic fields than a typical neutron star and have longer spin periods. These are relatively rare, with only 30 magnetars being confirmed so far.

2. Pulsars are neutron stars that emit prominent beams of electromagnetic radiation. In rapidly rotating neutron stars, the rotation of the magnetic field sets up an electrical field that accelerates protons and electrons from the star's surface to form a beam of electromagnetic radiation emitted from the star's magnetic poles. These poles need not be aligned with the rotational axis of their neutron star. Thus, during observation, the beam appears to be swept around the neutron star at regular intervals, similar to

a lighthouse signal. Most neutron stars discovered so far have been pulsars or related objects.

Pulsars with less than ten millisecond spin periods are termed Millisecond pulsars (MSPs).

0.2 MSP Formation

MSPs are typically old neutron stars that have undergone a form of 'recycling' to reach spin periods of the order of milliseconds. The current model of recycling is as follows:

Infalling matter gets channeled onto an accretion disk that surrounds the star. This accretion disc extends inward until it is stopped by the star's magnetosphere at what is known as its magnetospheric radius (r_m).

$$r_m = \xi(\frac{\mu^4}{2GM\dot{M}^2})^{\frac{1}{7}} \tag{1}$$

where G is the gravitational constant, $\dot{M}$ is the accretion rate, μ is the magnetic dipole moment of the star, and ξ is a constant (of order unity) that depends on the threading of the neutron star by magnetic field lines. A neutron star can accrete mass and angular momentum onto the surface when its magnetospheric radius is lesser than its corotation radius (r_{co}). This is the radius at which an orbiting object's Keplerian velocity equals the neutron star's rotational velocity.

$$r_{co} = (\frac{GM}{4\pi^2\nu^2})^{\frac{1}{3}} \tag{2}$$

This is known as the "accretion regime." The matter gets channeled to the star's magnetic poles, causing it to spin up and emit X-ray pulsations. As it spins up, the corotation radius shrinks, moving closer to the magnetospheric radius. Eventually, once the corotation radius shrinks beyond the magnetospheric radius, no more matter can be accreted onto the neutron star's surface. [14].

0.3 The transitional millisecond pulsar

Transitional millisecond pulsars (or tMSPs), as the name suggests, are a class of objects that are characterized mainly by the fact that they're in a sort of "transition state" between a rotational millisecond pulsar (RMSP) and an accretion-powered low-mass X-ray binary (LMXB). Observations show that these sources switch between these two states on a multi-year timescale. [6].
There are currently three known tMSPs: PSR J1023+0038 [6], XSS J12270–4859 [8], and IGR J18245–2452 [20]. PSR J1023+0038 (henceforth J1023) is a well-studied tMSP owing to its relatively close distance from us [15].

The existence of tMSPs invites questions like how does the transition between LMXB and RMSP states occur? How does the star's accretion take place during the LMXB state? Additionally, studying these objects can shed crucial light on better understanding the recycling mechanisms that govern MSP formation [17].

0.4 The history of J1023

J1023 was first discovered in August 1998 in the FIRST VLA 1.4 GHz continuum radio sky survey [9]. Observations in March 1999 [25] showed its similarity to a G star.
J1023 showed a stark change in its spectra when observed in May 2000; however, [12] with the spectrum being substantially bluer and the presence of emission lines. This led to its classification as a cataclysmic variable. Subsequent observations in 2001-2007 suggested the absence of an accretion disk. [6] This gave strong evidence that J-1023 had turned on to an RMSP state sometime between 2001-2007. Due to its well-observed state transitions, J1023 has been called a 'missing link' in the evolutionary cycle of MSPs [19].
J1023 remained in an RMSP state from 2007 till 2013, when it switched off as a radio pulsar [23] and developed an accretion disk [22]. J1023 currently exists in its LMXB state.

While in the LMXB, J1023 displays stark switches in its brightness in its X-ray profile. These switches occur between three modes with different luminosities:

1. The high mode ($L_X \sim 10^{33} ergs^{-1}$), existing for ∼70%-80% of the state

2. The low mode ($L_X \sim 5 * 10^{32} ergs^{-1}$), existing for ∼20% of the state

3. Occasional flares ($L_X \sim 5 * 10^{34} ergs^{-1}$), accounting for 2%

Another phenomenon displayed by J1023 in the high mode is coherent X-ray pulsations. The spin-down rates of J1023 have been measured for both its states, namely $-1.89 * 10^{-15} Hzs^{-1}$ for the RMSP state and $-2.5 * 10^{-15} Hzs^{-1}$ for the LMXB state. Multiple attempts have been made to explain the change in the spin-down rate and the existence of X-ray pulsations in the high mode [24] [26] [21].

0.5 The possible ellipticity of J1023

Although many models exist that explain the various properties displayed by J1023, they fail to account for all the phenomena exhibited by this source. For example, some models explain the γ-ray luminosity of the LMXB state remarkably well but cannot explain the presence of stable X-ray modes and the X-ray pulsations observed in the high mode [24] [26]. Other models opt for a much higher neutron star accretion rate in the LMXB state [21], which propels nearly 99% of accreted matter away, but this implies spin-down rates at least twice as high as the ones observed. As mentioned in Bhattacharyya (2020) [10], these models do not account for any neutron star spin frequency changes that could arise from gravitational waves. This formalism adopts a physical picture of J1023 in which the star has an asymmetric distribution of mass around its spin axis, which results in the continuous emission of gravitational waves that affect the spin frequency of the star. Calculations conducted with this formalism show that the X-ray pulsations and accretion of matter onto the surface in the high mode are natural consequences. Hence, we conduct a comprehensive spectral analysis of J1023 to test for the accretion of matter onto its surface in the high mode.

0.6 The scope of the project

This project focuses on the spectral analysis of PSR J1023 to probe the accretion of matter onto its surface during the high mode. This would help verify the NS's ellipticity, which would imply the emission of continuous gravitational waves, a phenomenon that has not been observed so far[10].
We will probe the high-mode picture by looking at the inner radius of the accretion disk and verifying whether it lies within the corotation radius (consistent with the previously stated model for NS accretion).

Chapter 1

Data files and Software

1.1 The XMM-Newton EPIC Data

The XMM-Newton satellite carries three CCD cameras which comprise the European Photon Imaging Camera (EPIC). Two are Metal Oxide Semiconductors (MOS) CCD cameras, while the third uses a pn CCD. The EPIC cameras can perform extremely sensitive imaging observations over the telescope's field of view of 30 arcmins and in the energy range from 0.15 to 15 keV.

All three cameras operate in photon counting mode and produce event lists, i.e., tables with one entry line per received event. They also detail other properties, such as the position at which they were registered, their arrival time, and their energies.

This project analyzed data from the XMM-Newton satellite across multiple years. All data was sourced from the publicly available HEASARC archives using the HEASARC Browse Search Form [1]. A total of 18 observation directories were downloaded from the *xmmmasterlog* repository. The EPIC data is contained in the ODF folder within each directory.

Table 1.1: Observation Log

Obs. ID.	Obs. Start (DD-MM-YYYY)	Instrument	Duration (ks)	High State dur. - (ks)	Low State dur. - (ks)
0720030101	2013-11-10	pn (FT)	128.37	60.04	11.40
		MOS (SW)	128.88	69.61	13.09
0742610101	2014-06-10	pn (FT)	116.72	5.35	1.57
		MOS (SW)	118.49	6.31	1.83
0748390101	2014-11-21	pn (FT)	32.43	15.1	3.48
		MOS (SW)	34.32	17.1	3.88
0748390501	2014-11-23	pn (FT)	32.93	18.2	2.96
		MOS (SW)	34.81	20.4	3.32
0748390601	2014-11-28	pn (FT)	16.93	8.6	3.42
		MOS (SW)	20.62	9.75	3.85
0748390701	2014-12-17	pn (FT)	32.54	19.7	2.74
		MOS (SW)	34.42	22.2	3.08
0770581001	2015-11-11	pn (FT)	27.34	15.2	1.90
		MOS (SW)	29.22	17.3	2.13
0770581101	2015-11-13	pn (FT)	20.74	11.78	1.35
		MOS (SW)	22.62	13.19	1.57
0783330301	2015-12-09	pn (FT)	24.43	15.46	1.34
		MOS (SW)	26.32	17.01	1.59
0784700201	2016-05-08	pn (FT)	123.86	51.59	5.08
		MOS (SW)	116.41	59.32	5.86
0794580801	2017-05-23	pn (FT)	22.74	10.89	1.99
		MOS (SW)	24.61	12.42	2.33

Table 1.2: Observation Log (continued)

Obs. ID.	Obs. Start (DD-MM-YYYY)	Instrument	Duration (ks)	High State dur. - (ks)	Low State dur. - (ks)
0794580901	2017-05-24	pn (FT)	21.24	11.65	3.06
		MOS (SW)	23.11	12.44	3.29
0803620201	2017-05-08	pn (FT)	22.04	10.53	1.01
		MOS (SW)	23.91	11.70	1.08
0803620301	2017-05-10	pn (FT)	25.73	15.54	2.18
		MOS (SW)	27.61	17.26	2.42
0803620401	2017-05-16	pn (FT)	20.73	12.55	2.35
		MOS (SW)	22.61	13.77	2.46
0803620501	2017-06-13	pn (FT)	20.73	10.33	1.57
		MOS (SW)	22.61	11.16	1.70
0823750301	2018-12-11	pn (FT)	26.38	15.43	1.83
		MOS (SW)	28.61	17.49	2.00
0823750401	2018-12-15	pn (FT)	30.38	18.88	1.26
		MOS (SW)	32.61	20.72	1.46

1.2 The XMM-Newton CCF

Along with the XMM-Newton ODF data, it is necessary to download the repository of Current Calibration Files (CCF) from the XMM-Newton ESA webpage. [4]

1.3 The XMM Science Analysis Software

All the data downloaded from the XMM-Newton archives must be processed by the XMM Science Analysis Software (XMMSAS) to retrieve scientific products for analysis. This is a collection of scripts, libraries, and tasks specifically designed to reduce and analyze data from the XMM-Newton observatory.
The XMMSAS can be downloaded from their official website [4] and installed following the guide mentioned therein.
The XMMSAS version 20.0.0 was used for the work of this project.

1.4 HeaSoft

HeaSoft is a unified release of the FTOOLs and XANADU software packages [2], and consists of the following :

1. XANADU - A package that helps with spectral, timing, and imaging data analysis
2. FTOOLS - A package that contains multiple tools to process FITS files
3. FITSIO - The core library responsible for reading and writing FITS files
4. fv - A software that can browse, edit, and plot FITS files with a GUI
5. XSTAR - A tool for calculating the physical conditions and emission spectra of photo-ionized gases

Of the aforementioned software, the package within XANADU that deals with high-level X-ray astronomical spectral data analysis, namely XSPEC, will be of utmost importance in analyzing and modeling spectral products.

1.5 Miscellaneous

Apart from the mission and task-specific software, this project also utilized basic coding in Python to read/write tables and generate sorting algorithms to filter out data sets of interest.

The visualization tool *SAOImageDS9* was also used to image satellite data and to select the source and background region.

Chapter 2

Data Analysis

2.1 Setting up the XMMSAS environment

2.1.1 Initialising HEADAS

To start up the XMMSAS, we must call upon the *headas-init.sh* file within the installation directory. This involves the definition of a variable that points to the file directory. Once this variable has been defined, it must be used to execute a shell script.

export HEADAS=path to *headas-init.sh* (e.g./usr/local/heasoft-M.N.P/....)
. $HEADAS/headas-init.sh

2.1.2 Initialising SAS

In a similar process to the initialization of HEADAS, we must invoke the *setsas.sh* file to initialize the XMMSAS. This must be done precisely as mentioned before in 2.1.1.

export SAS_DIR=/some_dir/xmmsas_20211110_1931
. $SAS_DIR/setsas.sh

2.1.3 The Calibration Files

Then next step is specifying the location of the XMM-Newton CCF. This is done by defining an environment variable known as SAS_CCFPATH.

export SAS_CCFPATH=path to CCF (e.g./usr/local/ccf)

2.1.4 The Observation Data Files

In this step, we must specify the location of the ODF folder of the XMM-Newton observation under study. The environment variable for this is SAS_ODF.

export SAS_ODF=path to ODF folder (e.g./home/user/xmm_obs/0099280201)

2.1.5 Producing the Calibration Index File

Before processing the data set present in the ODF folder, we must run a task to identify which specific calibration files will be necessary for analysis. This is carried out by issuing the *cifbuild* command.
The *cifbuild* command will access the ODF through SAS_ODF and look at all the calibration files in SAS_CCF to determine which files are necessary. The command generates an output file denoted by *ccf.cif* in the directory where the command was run.
Once the *ccf.cif* is generated, the SAS_CCF variable must be re-assigned to point at it instead.

export SAS_CCF='pwd'/ccf.cif

2.1.6 The ODF summary file

Within the ODF folder of any XMM-Newton observation, there is a summary file of all the observational data. Before processing data with SAS, it is necessary to update this summary file.

The command *odfingest* does this task. By simply running it with no argument, it generates an updated summary file in one's working directory. After completing the task, the variable SAS_ODF must be reassigned to point toward this.

export SAS_ODF=‘pwd‘/‘ls -1 *SUM.SAS‘

This concludes the setting up of the XMMSAS environment. We may now proceed with reducing the data of the MOS1 and MOS2 CCDs.

2.2 The MOS Analysis

2.2.1 Foreword

The re-processing, filtering, and cleaning of all XMM-Newton data have been carried out by the protocol depicted in the following flowchart. Each stage refers to a new file being generated.

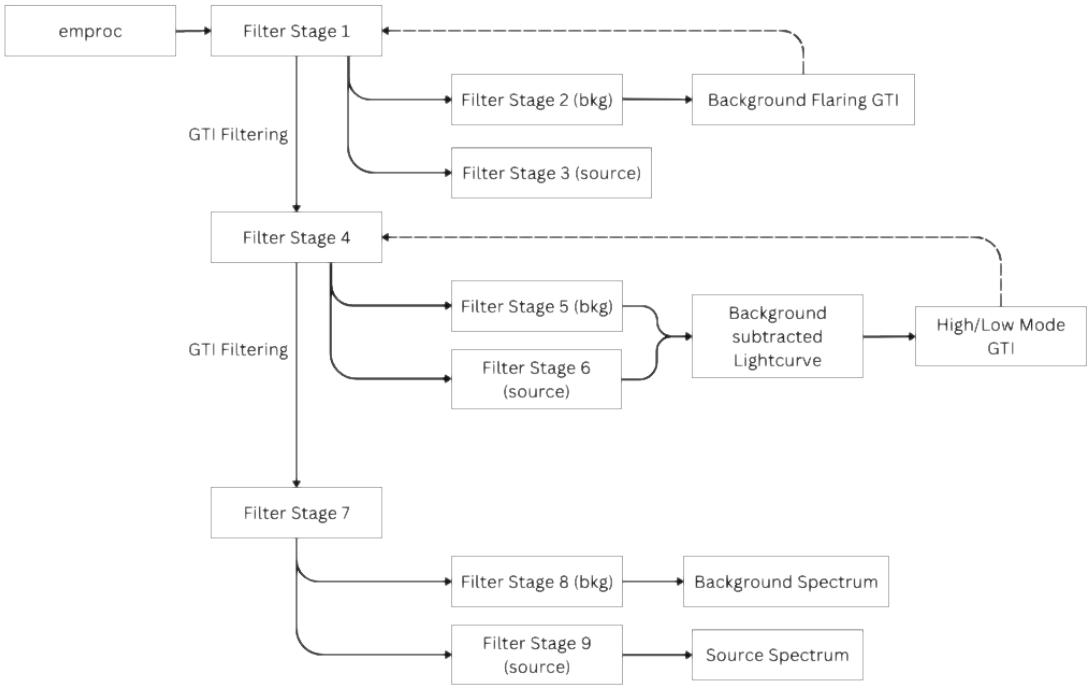

Figure 2.1: Pipeline of MOS data Analysis

2.2.2 Re-processing and filtering of data

The XMMSAS command *emproc* was used to re-process the ODF data to generate the event lists of the MOS1 and MOS2 CCDs. For all MOS data, we filtered our files using pattern 0-12, and the FLAG==0 and #XMMEA_EM options.

In the case of any flares present in the data, the filtering was carried out in keeping with the protocol of the XMMSAS User Analysis Thread [4].

2.2.3 Checking for background flaring

We begin the filtering pipeline by running a basic filtering criterion using #XMMEA_EM and constraining the energy range within 200eV to 12keV (PI in [200:1200]) The resultant filtered file termed as *Filter Stage 1* is then visualized using SAOImageDS9 to select the source and background regions.

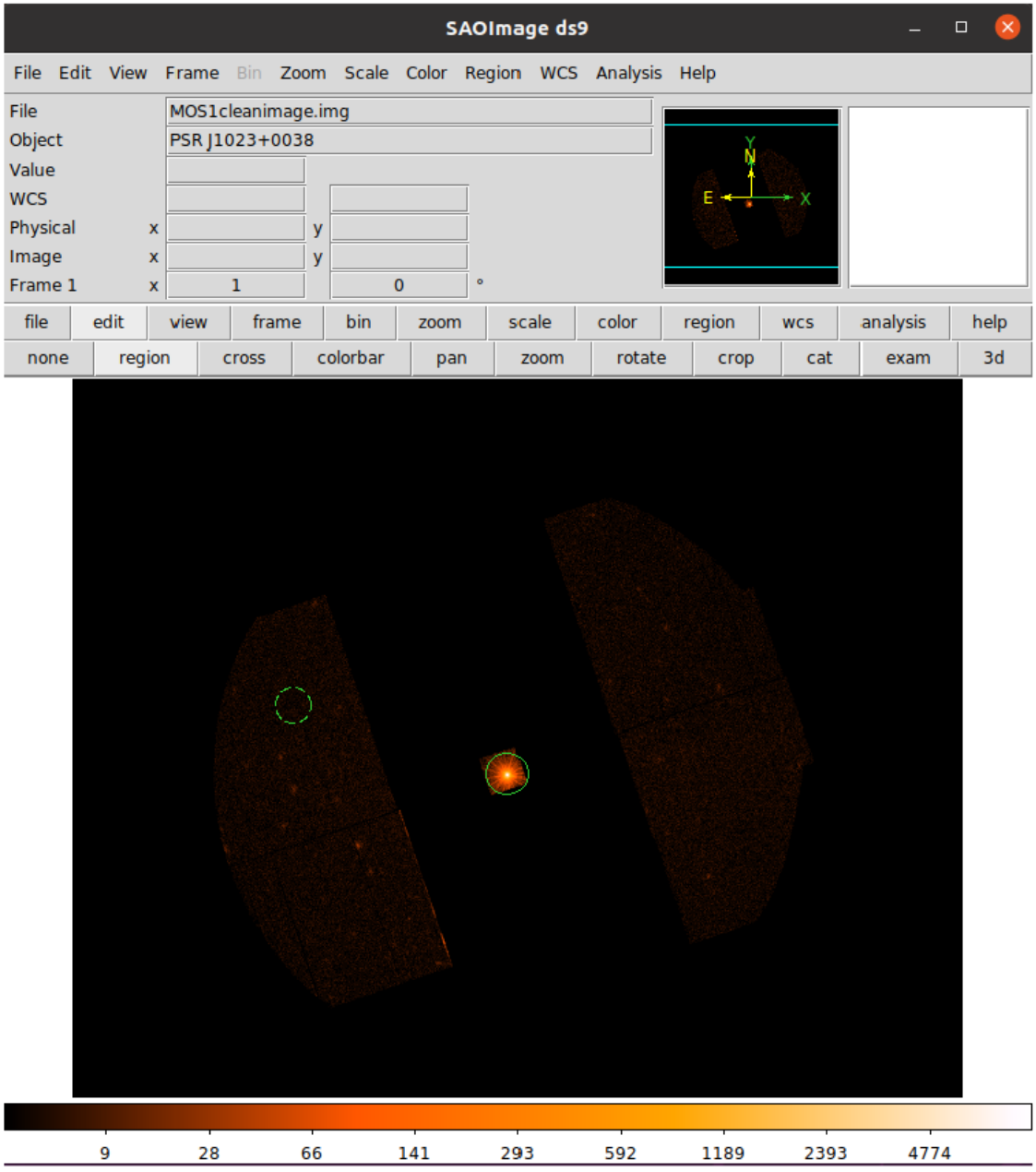

Figure 2.2: Screenshot of MOS data visualization - Source and background regions specified

All MOS data was recorded in the small-window sky-imaging mode. This means that the image is displayed using the physical X and Y coordinates, with four large panels blocking the immediate surroundings of the source to ensure no background interferes with it. The background region is chosen to be as large as possible to ensure minimum random errors.

The background and source regions are then extracted from *Filter Stage 1*, becoming files *Filter Stage 2* and *Filter Stage 3*, respectively. We generate a light curve of the background region using the *evselect* command with *withrateset=yes*. This enables us to observe whether the background has any flaring activity which might affect our source.

2.2.4 Filtering out flaring activity using GTIs

Depending on the presence of a flaring background, a good time interval (GTI) would be generated using the *gtiset* command. This GTI would specify all the time points of flares in the background light curve. These time points would then be screened out of *Filter Stage 1* to produce the background flaring cleaned file, *Filter Stage 4*. (Refer to Section 6.2.4 in The XMM-Newton ABC Guide[3] for more information on time-filtering using GTIs)

2.2.5 Generating a background subtracted, exposure corrected source lightcurve

Using the cleaned event file *Filter Stage 4*, we generate a background-subtracted exposure corrected light curve of the source. This light curve depicts the behavior of our source without the interference of any background flaring effects. This is done by running the *xmmselect* command with *rateset* and also running the *epiclccorr* command specifying the source, background, and raw data files to carry out background subtraction and exposure correction. The data from all three CCDs, namely MOS1, MOS2, and pn, are co-added using *lcmath* in the *Heasoft* package.

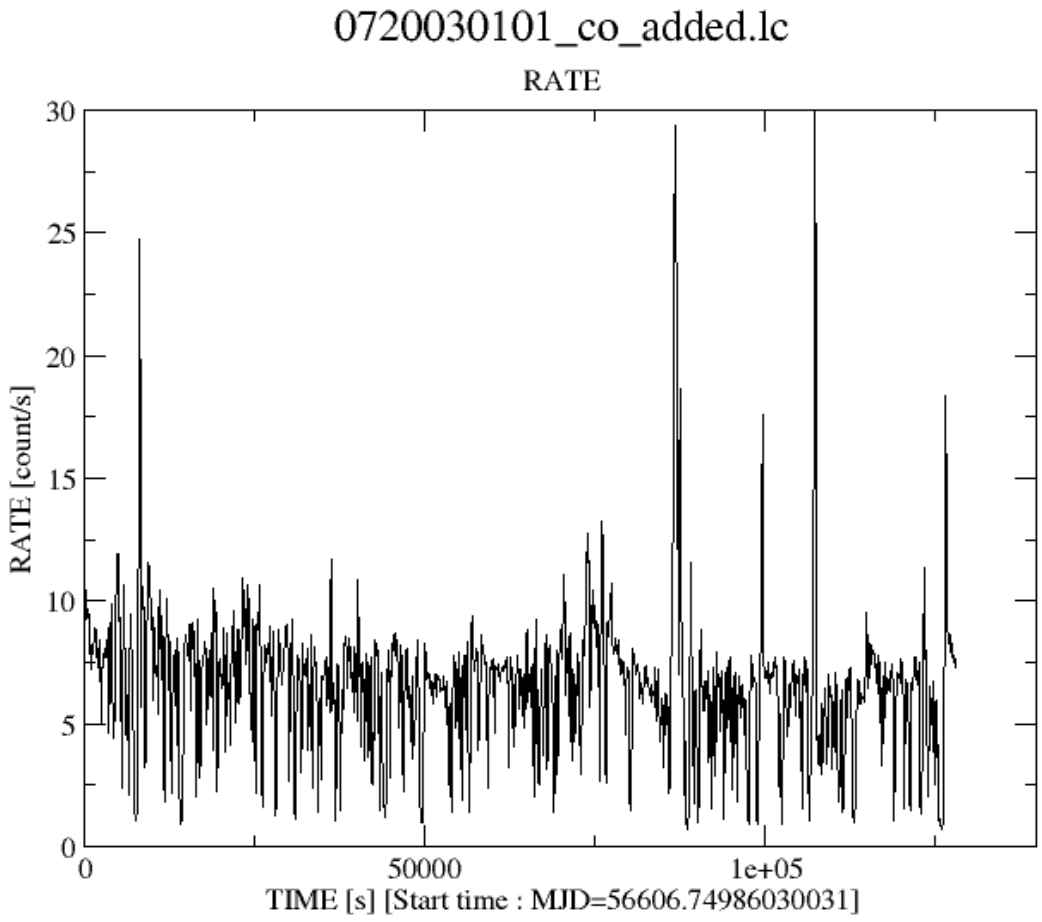

Figure 2.3: Background subtracted, exposure corrected, and total co-added lightcurve of the OBS ID 0720030101

Using this light curve, we can generate two new good time intervals, one where the source is purely in the high mode and one where the source is purely in the low mode. This is carried out using *gtiset* while selecting time points where the count rate of the source lies within [4.1,11]ct/s for the high mode and [0,2.1]ct/s for the low mode. The specifications for the high mode and low mode count rates were taken in keeping with that of *Campana et al.* [13].

2.2.6 Separating the High and Low modes

By using the high and low mode GTIs as the filtering criterion on *Filter Stage 4*, we arrive at our *Filter Stage 7*. Two files are generated at this stage - one for purely high-mode data and one for purely low-mode data. We proceed with the description of only the high-mode data analysis, keeping in mind that the same is carried out for the low-mode.

2.2.7 Generating the source and background spectra

Using the filtered high-mode data, we use the same region extraction specifications to generate background and source filtered files, named *Filter Stage 8* and *Filter Stage 9* respectively. We then use the *evselect* command with *spectrumset=yes* on these files to produce the background and source spectrum files.
Additionally, we also generate redistribution matrix files (RMFs) using *rmfgen* and ancillary response files (ARFs) using *arfgen*.
The MOS spectra are combined using *epicspeccombine* in *Heasoft*, and the resultant combined source spectrum is re-binned to have a minimum of 100 counts in each bin. For the low mode, the combined source spectrum is re-binned to have a minimum of 20 counts per bin instead.

2.3 Loading the files into XSPEC

Once the combined source spectrum is generated, we upload the files into XSPEC. The re-binned source spectrum, the background spectrum, and the response files (ARF and RMF) are loaded into the XSPEC instance.
The x-axis is defined in eV units, and the spectrum is restricted to only display channels within 300eV-10keV. All MOS spectra of the 18 observations are summed up to produce one total MOS spectral file.

Chapter 3

Spectral Modeling and Fitting

3.1 The Model

For our spectral fitting, we modified a model presented in *Campana et al.* [13] and used it in our data analysis.
The model we used to fit our data is described as follows:

$$TBabs * (powerlaw + diskbb + nsatmos) \tag{3.1}$$

This is a composite model made up of the following components:

1. *TBabs*: The Tuebingen-Boulder ISM absorption model. This is a model used for the calculation of X-ray absorption of Interstellar Medium (ISM).
2. *powerlaw*: The simple photon power law.
3. *diskbb*: An model for an accretion disk with multiple blackbody components.
4. *nsatmos*: The NS Hydrogen Atmosphere model used to model the heated polar cap of the neutron star.

All model components and their descriptions are mentioned in the XSPEC User Guide. Refer to [5] for more information.

3.2 Fixed Parameters

Within XSPEC, we restrict the variation of certain parameters in our model to not arrive at an unphysical result. The source is known to be at a distance of 1.37kpc from Earth; hence, the *dist* parameter in *nsatmos* is frozen to a value of 1.37.
Additionally, we redefine the parameter of neutron star mass M_{ns} to lie within the range of 1.4-2.2 solar masses.

Chapter 4

Results

4.1 The Spectral Fit

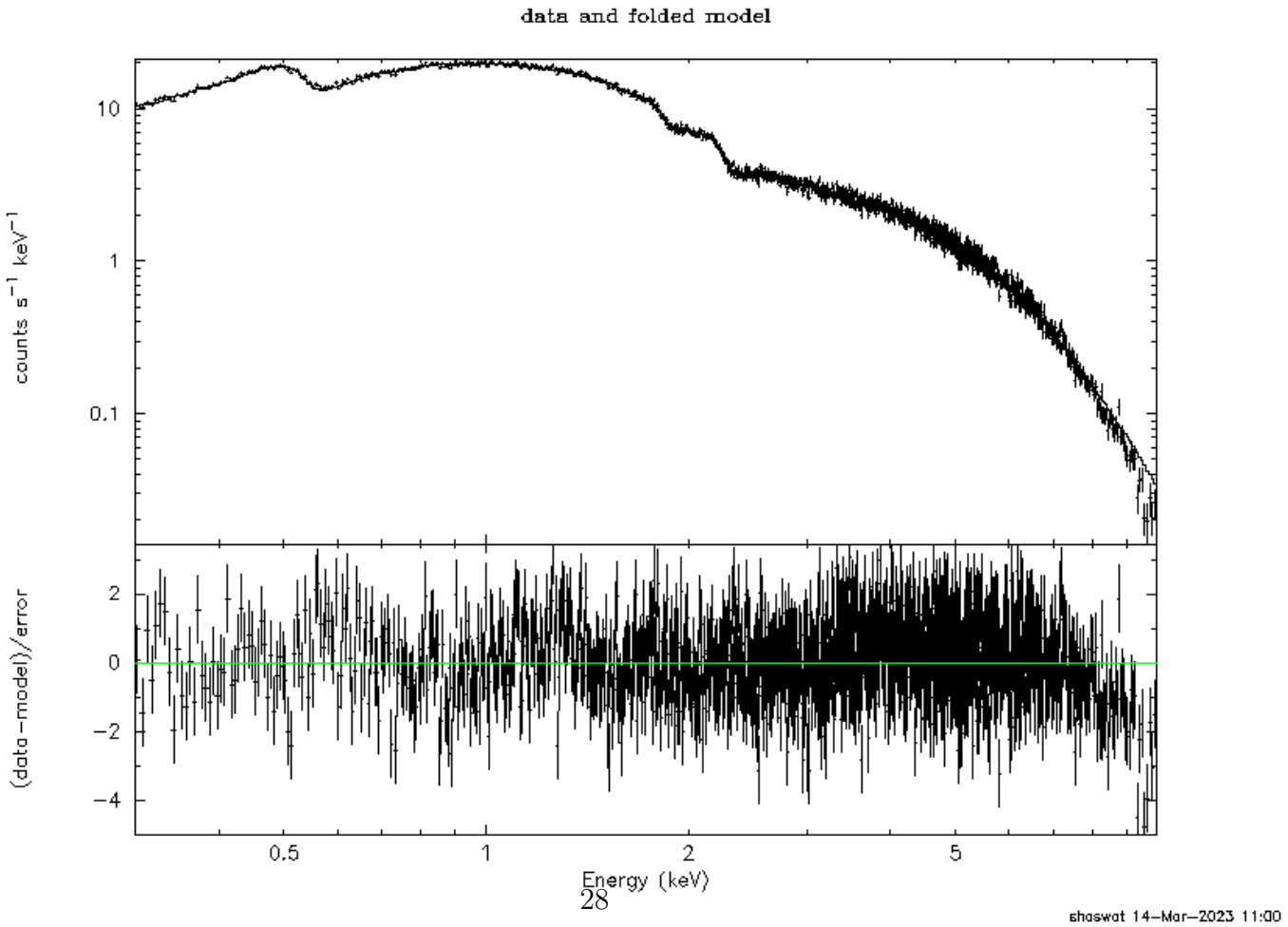

Figure 4.1: Spectral Fit for the MOS summed up spectra for the high mode

Table 4.1: High Mode Spectral Fits ($red.\chi^2 = 1.02$ with 1247 $dof.$ and systematic error of 2%)

Spectral Parameter	High Mode
N_H (10^{20} cm^{-2})	4.105 ± 0.2
Power law Γ_D	$1.611^{+0.005}_{-0.007}$
Power law N_D (10^{-4})	$16.071^{+0.135}_{-0.167}$
Disc T (eV)	108^{+12}_{-10}
Disc norm. N_d	297^{+227}_{-131}
log(T_{eff})	$6.201^{+0.23}_{-0.15}$
nsatmos norm.	$0.0391^{+0.441}_{-0.026}$

We obtain a reduced $\chi^2 = 1.02$ for the fit with 1247 degrees of freedom while accounting for a systematic error of 2%. The error computation for the log(T_{eff}) failed for the upper limit, possibly due to attaining the maximum limit value.
The importance of the disk component (*diskbb*) is confirmed with F-test value = 121.298 and probability = 7.31763 * 10^{-49}. The high F-test value suggests that adding this component to our model greatly increased the quality of our fit. This is in agreement with Campana *et al.* (2016) [13].

The disc norm, which is the value we are primarily concerned with, displays a large variation ranging from 133 to 524. This, however, is within the same order as that published in other literature [13] [27].

4.2 Calculations

To compute the inner radius of the disc, we use the formula mentioned in the XSPEC manual [5]. The disc norm is related to the "apparent" inner radius (r_{in}) as follows :

$$r_{in} = \sqrt{\frac{Norm}{cos\theta}} * D_{10} \tag{4.1}$$

where θ is the angle of inclination of the disc, and D_{10} is the distance of the star in units of 10kpc.
We know that $\theta = 42°$ [6] and $D_{10} = 0.137$. Plugging this into our calculations, we can obtain the range of our apparent inner disc radius to be [2.051, 3.645] km.

The apparent inner radius is related to the *true* inner radius (R_{in}) as:

$$R_{in} = \xi * \kappa^2 * r_{in} \tag{4.2}$$

$\xi \sim 1$ and $\kappa \sim 2$ [18]. This yields us the estimate of the true inner radius to be around [8.2, 14.58] km. This is well within the co-rotation radius of 24km.

4.3 Errors

4.3.1 Error Calculation

Error calculation was carried out within XSPEC using the *error* command. Each parameter was varied within their respective hard limits until the value of the fit statistic lies within a tolerance interval of 0.01 of the previous fit statistic plus the σ value (in our case, $\sigma = 2.706$). In certain scenarios, the error calculations would fail due to attaining a hard limit or the fit not converging to the desired value. In such cases, the parameter was redefined to lie in a new range while ensuring the values obtained were still physical.

4.3.2 Uncertainties in Analysis

The processing of raw MOS data involved the selection of source and background regions for spectral products. This process bore a reasonable amount of uncertainty due to the background regions possessing great deals of variability across multiple years.
To minimize selection bias, we chose as large a background region as possible from each observation ID and screened it to remove any flares.

4.4 Discussion

Although we report the results obtained from fitting our model to the combined MOS spectra of 18 observations, we also fit the same model to each observation separately to observe the presence of any trends. We performed a separate spectral fitting of 3 long observations (obsID 0720030101, 0784700201, and 0742610101) and observed similar parameters.
The parameters obtained for the spectral fit of the inner disk radius, coupled with the high luminosity ($L_x \sim 10^{33} ergs$), strongly suggest that matter is channeled onto the neutron star's surface in the high mode. Our spectral fits are of the same order of magnitude as those reported by Campana *et. al.* [13] and Zelati *et. al.* [27] although our disc parameters display considerably higher variation.
Concerning whether this might support the ellipticity of J1023, the formalism adopted in Bhattacharyya (2020) [10], the channeling of matter onto the NS surface is a natural consequence of its ellipticity. Our results provide a compelling argument for its existence.
Going forward, the ellipticity of J1023 opens up new avenues for research into its structure and properties. The continuous emission of gravitational waves by J1023 due to its ellipticity will be a topic bearing great promise. Further analysis of J1023 can be done using data from other satellites such as NICER and Chandra, which would help strengthen our foundational knowledge on this source.

Chapter 5

Conclusion and outlook

We performed the spectral analysis of PSR J1023+0038 using data from 18 observations. We have found that the accretion disk model holds very well in explaining the high mode behavior of J1023 in its LMXB state. The results obtained in this project motivate the existence of a permanent ellipticity in the neutron star. This provides evidence for a non-trivial contribution of continuous gravitational wave emission in the changes of neutron star spin-down rate between the RMSP and LMXB states. The accretion disk model successfully explains the X-ray pulsations in the high mode, and the calculations of the co-rotation and magnetospheric radius indicate that matter is channeled onto the neutron star magnetic poles.

Bibliography

[1] *Heasarc browse: Main interface.*

[2] *Heasoft - download (version 6.31).*

[3] *The xmm-newton abc guide: an introduction to xmm-newton data analysis.*

[4] *Xmm-newton soc home page (www.cosmos.esa.int).*

[5] *Xspecmanual.*

[6] A. M. Archibald, I. H. Stairs, S. M. Ransom, V. M. Kaspi, V. I. Kondratiev, D. R. Lorimer, M. A. McLaughlin, J. Boyles, J. W. T. Hessels, R. Lynch, J. van Leeuwen, M. S. E. Roberts, F. Jenet, D. J. Champion, R. Rosen, B. N. Barlow, B. H. Dunlap, and R. A. Remillard, *A Radio Pulsar/X-ray Binary Link*, Science, 324 (2009), p. 1411.

[7] J. Bally and B. Reipurth, *The birth of stars and planets*, University Press, 2006.

[8] C. G. Bassa, A. Patruno, J. W. T. Hessels, E. F. Keane, B. Monard, E. K. Mahony, S. Bogdanov, S. Corbel, P. G. Edwards, A. M. Archibald, G. H. Janssen, B. W. Stappers, and S. Tendulkar, *A state change in the low-mass X-ray binary XSS J12270-4859*, , 441 (2014), pp. 1825–1830.

[9] R. H. Becker, R. L. White, and D. J. Helfand, *The FIRST Survey: Faint Images of the Radio Sky at Twenty Centimeters*, , 450 (1995), p. 559.

[10] S. Bhattacharyya, *The permanent ellipticity of the neutron star in PSR j10230038*, Monthly Notices of the Royal Astronomical Society, 498 (2020), pp. 728–736.

[11] I. Bombaci, *The maximum mass of a neutron star.*, , 305 (1996), p. 871.

[12] H. Bond, R. White, R. Becker, and M. O'Brien, *First j102347.6+003841: The first radio-selected cataclysmic variable*, Publications of the Astronomical Society of the Pacific, 114 (2002), pp. 1359–1363.

[13] S. Campana, F. C. Zelati, A. Papitto, N. Rea, D. F. Torres, M. C. Baglio, and P. D'Avanzo, *A physical scenario for the high and low x-ray luminosity states in the transitional pulsar PSR j10230038*, Astronomy & Astrophysics, 594 (2016), p. A31.

[14] F. D'Antona and M. Tailo, *Origin and binary evolution of millisecond pulsars*, 2020.

[15] A. T. Deller, A. M. Archibald, W. F. Brisken, S. Chatterjee, G. H. Janssen, V. M. Kaspi, D. Lorimer, A. G. Lyne, M. A. McLaughlin, S. Ransom, I. H. Stairs, and B. Stappers, *A PARALLAX DISTANCE AND MASS ESTIMATE FOR THE TRANSITIONAL MILLISECOND PULSAR SYSTEM j10230038*, The Astrophysical Journal, 756 (2012), p. L25.

[16] A. Heger, C. L. Fryer, S. E. Woosley, N. Langer, and D. H. Hartmann, *How Massive Single Stars End Their Life*, , 591 (2003), pp. 288–300.

[17] A. Jaodand, A. M. Archibald, J. W. Hessels, S. Bogdanov, C. R. D'Angelo, A. Patruno, C. Bassa, and A. T. Deller, *Timing observations of psr j1023+ 0038 during a low-mass x-ray binary state*, The Astrophysical Journal, 830 (2016), p. 122.

[18] A. Kubota, Y. Tanaka, K. Makishima, Y. Ueda, T. Dotani, H. Inoue, and K. Yamaoka, *Evidence for a Black Hole in the X-Ray Transient GRS 1009-45*, , 50 (1998), pp. 667–673.

[19] D. Lorimer, *PSR J1023+0038: Tracing the Accretion History of a "Missing Link'*. Chandra proposal ID 11400764, Sept. 2009.

[20] A. Papitto, C. Ferrigno, E. Bozzo, N. Rea, L. Pavan, L. Burderi, M. Burgay, S. Campana, T. di Salvo, M. Falanga, M. D. Filipović, P. C. C. Freire, J. W. T. Hessels, A. Possenti, S. M. Ransom, A. Riggio, P. Romano, J. M. Sarkissian, I. H. Stairs, L. Stella, D. F. Torres, M. H. Wieringa, and G. F. Wong, *Swings between rotation and accretion power in a binary millisecond pulsar*, , 501 (2013), pp. 517–520.

[21] A. Papitto and D. F. Torres, *A propeller model for the sub-luminous state of the transitional millisecond pulsar psr j1023+0038*, The Astrophysical Journal, 807 (2015), p. 33.

[22] A. Patruno, A. M. Archibald, J. W. T. Hessels, S. Bogdanov, B. W. Stappers, C. G. Bassa, G. H. Janssen, V. M. Kaspi, S. Tendulkar, and A. G. Lyne, *A NEW ACCRETION DISK AROUND THE MISSING LINK BINARY SYSTEM PSR j10230038*, The Astrophysical Journal, 781 (2013), p. L3.

[23] B. W. Stappers, A. Archibald, C. Bassa, J. Hessels, G. Janssen, V. Kaspi, A. Lyne, A. Patruno, and A. B. Hill, *State-change in the "transition" binary millisecond pulsar J1023+0038*, The Astronomer's Telegram, 5513 (2013), p. 1.

[24] B. W. Stappers, A. M. Archibald, J. W. T. Hessels, C. G. Bassa, S. Bogdanov, G. H. Janssen, V. M. Kaspi, A. G. Lyne, A. Patruno, S. Tendulkar, A. B. Hill, and T. Glanzman, *A state change in the missing link binary pulsar system psr j1023+0038*, The Astrophysical Journal, 790 (2014), p. 39.

[25] P. Szkody, O. Fraser, N. Silvestri, A. Henden, S. F. Anderson, J. Frith, B. Lawton, E. Owens, S. Raymond, G. Schmidt, M. Wolfe, J. Bochanski, K. Covey, H. Harris, S. Hawley, G. R. Knapp, B. Margon, W. Voges, L. Walkowicz, J. Brinkmann, and D. Q. Lamb, *Cataclysmic variables from the sloan digital sky survey. ii. the second year**, The Astronomical Journal, 126 (2003), p. 1499.

[26] J. Takata, K. L. Li, G. C. K. Leung, A. K. H. Kong, P. H. T. Tam, C. Y. Hui, E. M. H. Wu, Y. Xing, Y. Cao, S. Tang, Z. Wang, and K. S. Cheng, *Multi-wavelength emissions from the millisecond pulsar binary psr j1023+0038 during an accretion active state*, The Astrophysical Journal, 785 (2014), p. 131.

[27] F. C. Zelati, S. Campana, V. Braito, M. C. Baglio, P. D'Avanzo, N. Rea, and D. F. Torres, *Simultaneous broadband observations and high-resolution x-ray spectroscopy of the transitional millisecond pulsar PSR j10230038*, Astronomy &amp Astrophysics, 611 (2018), p. A14.